# Determination of virus burst size *in vivo* using a single-cycle SIV in rhesus macaques

Hannah Yuan Chen[†], Michele Di Mascio[‡], Alan S. Perelson[§], David D. Ho[†], and Linqi Zhang[†¶‖]

[†]Aaron Diamond AIDS Research Center, The Rockefeller University, 455 First Avenue, New York, NY 10016; [‡]National Institute of Allergy and Infectious Diseases, National Institutes of Health, 6700 B Rockledge Drive, MSC 7609, Bethesda, MD 20892; [§]Theoretical Division, Los Alamos National Laboratory, Los Alamos, NM 87545; and [¶]AIDS Research Center, Institute of Pathogen Biology, Chinese Academy of Medical Sciences and Peking Union Medical College, Tsinghua University, Beijing 100730, China

A single-cycle simian immunodeficiency virus (scSIV) that undergoes only one round of infection and replication was constructed to calculate the total number of virons produced by an SIV-infected cell *in vivo*. Four Mamu-A*01 rhesus macaques were inoculated on two occasions 11 weeks apart with the scSIV by *ex vivo* infection and i.v. reinfusion of autologous cells. After each inoculation, plasma viral loads peaked between 1 and 2.5 days and then declined exponentially in one or two phases to below detection limits within 2 weeks. Although higher levels of SIV-specific cytotoxic T lymphocytes and modest increases in antibody responses were observed for each animal after the second inoculation, decay rates of the infected cells were only minimally affected. Analyzing the viral load data with a mathematical model, the *in vivo* viral burst size averaged $4.0 \times 10^4$ and $5.5 \times 10^4$ virions per cell for the first and second inoculations, respectively, with no significant difference between the two inoculations. This estimate, in conjunction with our prior understanding of other quantitative viral and cellular parameters during SIV and HIV infection, provides critical insights into the dynamic process of viral production and its interplay with the infected host *in vivo*.

dynamic | HIV

The measurement of HIV and simian immunodeficiency virus (SIV) dynamic parameters through mathematical modeling has provided important insights into the virus–host relationship. One key viral dynamic parameter that remains ambiguous is the *in vivo* viral burst size, i.e., the total number of virions produced by an infected cell during its lifetime. Current HIV burst size estimates rely on either viral inhibitors, washouts of infected cells, or serial dilutions of infected cells to control for multiple rounds of infection (1–3). Alternatively, quantitative image analyses with *in situ* hybridization and quantitative, competitive RT-PCR of bulk tissue or single cells at limiting dilution (4–6) provide only transient "snapshots" of the infected cells, which may greatly underestimate this value.

To better determine the viral burst size *in vivo*, we used a single-cycle SIV (scSIV) that undergoes only one round of infection and replication (Fig. 1). This strategy enabled the determination of specific viral dynamic parameters *in vivo* without the confounding effects of subsequent viral spread and production. Our previous studies have shown that exogenously infused SIV particles into rhesus macaques and free HIV-1 virions in HIV-1-infected individuals are cleared rapidly from the plasma (7, 8). Such rapid clearance posed a challenge in the use of nonreplicating viral particles for *in vivo* dynamic studies in that these directly inoculated particles may be cleared before sufficient numbers of cells are infected. In addition, calculating the burst size from such experiments required an estimate of the rate of infection. Therefore, an infection strategy of first coculturing the scSIV particles *ex vivo* with peripheral mononuclear cells (PBMCs) isolated from rhesus macaques and then autologously reinfusing the cells by i.v. injection was adopted. This strategy ensured that sufficient numbers of cells would be infected before particle clearance and eliminated the necessity of the infection rate constant for burst size calculations
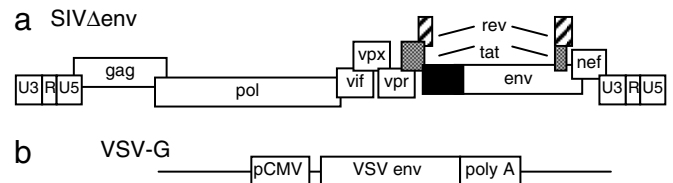


Fig. 1. Plasmid constructs used to generate scSIV. (*a*) SIVΔenv contains the SIVmac239 proviral genome with a 415-bp deletion at the 5′ end of the *env* gene. The black box indicates deleted sequences. (*b*) VSV-G contains the *env* gene of the VSV. Infectious scSIV were generated by cotransfecting 293T cells with the SIVΔenv and the VSV-G plasmids. Western blot analysis of the protein expression profile in both transfected cells and culture supernatants revealed comparable patterns to those of the wild-type SIVmac239 except for the loss of the envelope glycoprotein gp130 and the addition of the 67-kDa VSV-G glycoprotein (data not shown). *In vitro* measurements of the scSIV particles in transfected cell supernatants indicated that initial infectivity was conferred by the intact VSV-G on the virion surface. Subsequent rounds of infection were not detected because of the defective *env* within the virion genome (data not shown).

because the number of infected cells could be measured. Furthermore, coculturing scSIV directly with PBMCs allowed a more targeted infection of lymphocytes despite the presence of the multitropic vesicular stomatitis virus G (VSV-G) on the virion surfaces.

## Results and Discussion

Four SIV-naïve rhesus macaques (T696, T181, T599, and T646) with the Mamu-A*01 MHC class I phenotype were inoculated with scSIV by *ex vivo* infection and i.v. reinfusion of autologous cells. A second infusion was carried out 11 weeks later to assess the impact of preexisting immunity on the decay rate of infected cells and the viral burst size. Before each infusion, the number of infected cells in the inoculums was measured by real-time PCR targeted at the SIV *gag* gene, which is critical for the subsequent calculation of the viral burst size. Despite the high titers of scSIV particles ($>10^8$) used in the infection step, the number of *ex vivo*-infected cells for each animal varied between $5.2 \times 10^4$ and $4.8 \times 10^6$ with an overall average of $1.7 \times 10^6$ (Table 1) for both inoculations. This variation was anticipated given the differences in cell susceptibility and activation. Interestingly, the number of *ex vivo*-infected PBMCs followed the same pattern for the two independent procedures (Table 1), reinforcing the notion that intrinsic properties of the cells may influence their susceptibility to infection.

MEDICAL SCIENCES

**Table 1. SIV burst size and viral dynamic parameters after first and second ScSIV inoculations**

| Macaque | No. of infected PBMCs | First-phase dynamics | | | Second phase dynamics | | | Estimated burst size, AUC (virions per cell) |
|---|---|---|---|---|---|---|---|---|
| | | Estimated decay rate, $\delta$ (day 1) | 95% C.I. | $t_{1/2,\delta\rho}$, half-lives (days) | Estimated decay rate, $\mu$ (day 2) | 95% C.I. | $t_{1/2,\mu}$, half-lives (days) | |
| T696–1st | $4.8 \times 10^6$ | 1.20 | (1.08–1.34) | 0.58 | 0.25 | (0.15–0.33) | 2.77 | $1.3 \times 10^4$ |
| T181–1st | $3.3 \times 10^6$ | 0.57 | (0.51–0.64) | 1.22 | 0.10 | (0.02–0.12) | 6.93 | $4.0 \times 10^4$ |
| T599–1st | $4.3 \times 10^6$ | 0.50 | (0.41–0.70) | 1.39 | | | | $5.9 \times 10^4$ |
| T646–1st | $1.9 \times 10^5$ | 1.25 | (0.84–1.90) | 0.55 | 0.19 | (0.00–0.33) | 3.65 | $4.7 \times 10^4$ |
| Mean ± SD | $3.1 \times 10^6$ | 0.88 ± 0.40 | | 0.92 ± 0.37 | 0.18 ± 0.08 | | 4.45 ± 2.19 | $4.0 \times 10^4$ |
| T696–2nd | $5.6 \times 10^5$ | 1.01 | (0.60–1.40) | 0.69 | | | | $1.5 \times 10^4$ |
| T181–2nd | $1.2 \times 10^5$ | 2.75 | (1.83–4.70) | 0.25 | 0.57 | (0.52–0.63) | 1.22 | $1.2 \times 10^5$ |
| T599–2nd | $3.0 \times 10^5$ | 0.54 | (0.41–0.76) | 1.28 | | | | $6.7 \times 10^4$ |
| T646–2nd | $5.2 \times 10^4$ | 1.06 | (0.54–1.58) | 0.65 | | | | $1.7 \times 10^4$ |
| Mean ± SD | $2.6 \times 10^5$ | 1.34 ± 0.97 | | 0.49 ± 0.43 | | | | $5.5 \times 10^4$ |

The number of infected PBMCs was determined by real-time PCR assay targeted at the proviral SIV *gag* gene.

Plasma viremia increased rapidly, peaking between 1 and 2.5 days, and exponentially declined in one or two phases to below the detection limit in all four macaques after both inoculations (Fig. 2). After the first inoculation, viral loads peaked at $3.3 \times 10^5$ to $1.1 \times 10^7$ RNA copies per ml. After the second inoculation, plasma viremia peaked at $3.3 \times 10^4$ to $1.1 \times 10^6$ RNA copies per ml. This lower range of peak viremia after the second inoculation most likely reflects the smaller number of productively infected cells that were infused into the macaques (Table 1).

SIV-specific cytotoxic T lymphocyte (CTL) responses to the p11c epitope of SIV Gag were readily detected in all four macaques. The percentage of tetramer$^+$ and CD8$^+$ T cells peaked at 0.06–1.13% after the first inoculation. Greater increases were found after the second inoculation, with peaks at 0.09–2.23% (Fig. 2a). For both inoculations, a positive correlation clearly exists between the increase in CTL responses and the decline in viral loads (Fig. 2a). Antibody responses to the SIV p27 antigen in all four macaques, however, were only modest, at best, with peak titers ranging from 50 to 100 dilutions after the first inoculation and slightly increased titers of 100–3,300 dilutions after the second inoculation (Fig. 2b). Virtually no responses were observed against the SIV gp130 glycoprotein after either inoculation, which is consistent with the defective *env* within the infused scSIV (data not shown).

The best-fit theoretical curves to the viral load changes after peak viremia were generated by using a nonlinear least-square method to estimate the decay rate of productively infected cells (Fig. 3). After the first inoculation, two phases of decay, probably representing a shorter and a longer-lived population of infected cells, best characterized the viral decay observed in three of the four animals. After the second inoculation, only one of the four animals exhibited a two-phase viral load decay, probably because of the lower levels of peak viremia, such that the SIV RNA levels may have declined below the detection limit before a second phase became evident. Estimates of the decay rate, $\delta$, of the shorter-lived population after the first inoculation ranged from 0.50 to 1.25 per day, with a mean of 0.88 per day (Table 1). Correspondingly, the mean half-life, $t_{1/2,\delta}$, of the infected cells was 0.92 day (Table 1). These values are consistent with the death rates of productively infected lymphocytes as determined by antiretroviral treatment studies in SIV-infected macaques (9) and HIV-1-infected patients (10, 11). The relatively longer-lived population had a mean decay rate estimate, $\mu$, of 0.18 per day ($n = 3$) (Table 1). After the second inoculation, a faster mean decay rate, $\delta$, of 1.34 per day, with a corresponding mean half-life, $t_{1/2,\delta}$, of 0.49 per day, was observed for the shorter-lived population. This change reflects the substantial increase in $\delta$ in one of the animals. Additional repeat experiments would help determine the validity of this increase in cell death rate after a second inoculation.

We applied a simple mathematical model based on computing the total number of virions produced and dividing by the total number of productively infected cells inoculated into each animal to estimate the SIV burst size *in vivo*. With this method, the SIV burst size ranged from $1.3 \times 10^4$ to $5.9 \times 10^4$, with a mean of $4.0 \times 10^4$ virions per infected cell for the first inoculation and from $1.5 \times 10^4$ to $1.2 \times 10^5$, with a mean of $5.5 \times 10^4$ virions per infected cell for the second inoculation (Table 1). The difference observed in the means of the estimates between the two inoculations was not statistically significant.

In further reflecting on the viral burst size presented here, several influencing factors should be considered (Table 2), which may have a significant impact on the estimates of viral burst size. First, the envelope of the scSIV was the multitropic VSV-G glycoprotein, whereas the envelope of both HIV and SIV are predominantly tropic for CD4$^+$ lymphocytes. *Ex vivo* infections of isolated PBMCs with scSIV, therefore, would cause many different types of lymphocytes to be infected, not just CD4$^+$ T cells. Without differentiating, our calculations simply included all infected cells and assumed that they all produced similar levels of virions. However, with apparent infection of non-CD4$^+$ T cells through the VSV-G envelope, the true burst size in CD4$^+$ T cells may have been underestimated because many cells in the PBMCs, such as monocytes, are intrinsically less suitable for viral replication. Additional experiments using only CD4$^+$ T cells for the *ex vivo* infection may lead to a more accurate estimate.

Second, the extent of cell activation in our experiment before infection may not accurately reflect the conditions *in vivo*. Although quiescent lymphocytes may be permissive for SIV or HIV infection *in vivo*, viral production *in vitro* is usually not supported without initial cellular activation (12–15). Because the scSIV infections in these experiments were performed *ex vivo*, isolated PBMCs were first activated by Staphylococcal enterotoxin B (SEB) to ensure productive infections. Such a high level of uniform activation, which typically does not occur *in vivo* especially during the early stages of infection (16), may result in an overestimate of viral burst size. In contrast, however, highly activated lymphocytes may also be cleared faster when they pass through the lungs, resulting in an underestimate of viral burst size.

Third, the real-time PCR assay used in this study quantified the copies of proviral DNA without clarifying the actual number of cells in which they were contained. Each proviral DNA detected through real-time PCR was assumed to equal one productively infected cell such that no cell contained multiple proviruses. Contrary to this assumption, superinfections have been reported, with infected cells carrying multiple copies of proviral DNA (17, 18). Furthermore, the high multiplicity of infection (MOI) used in these *ex vivo* infections would have favored the occurrence of superinfections
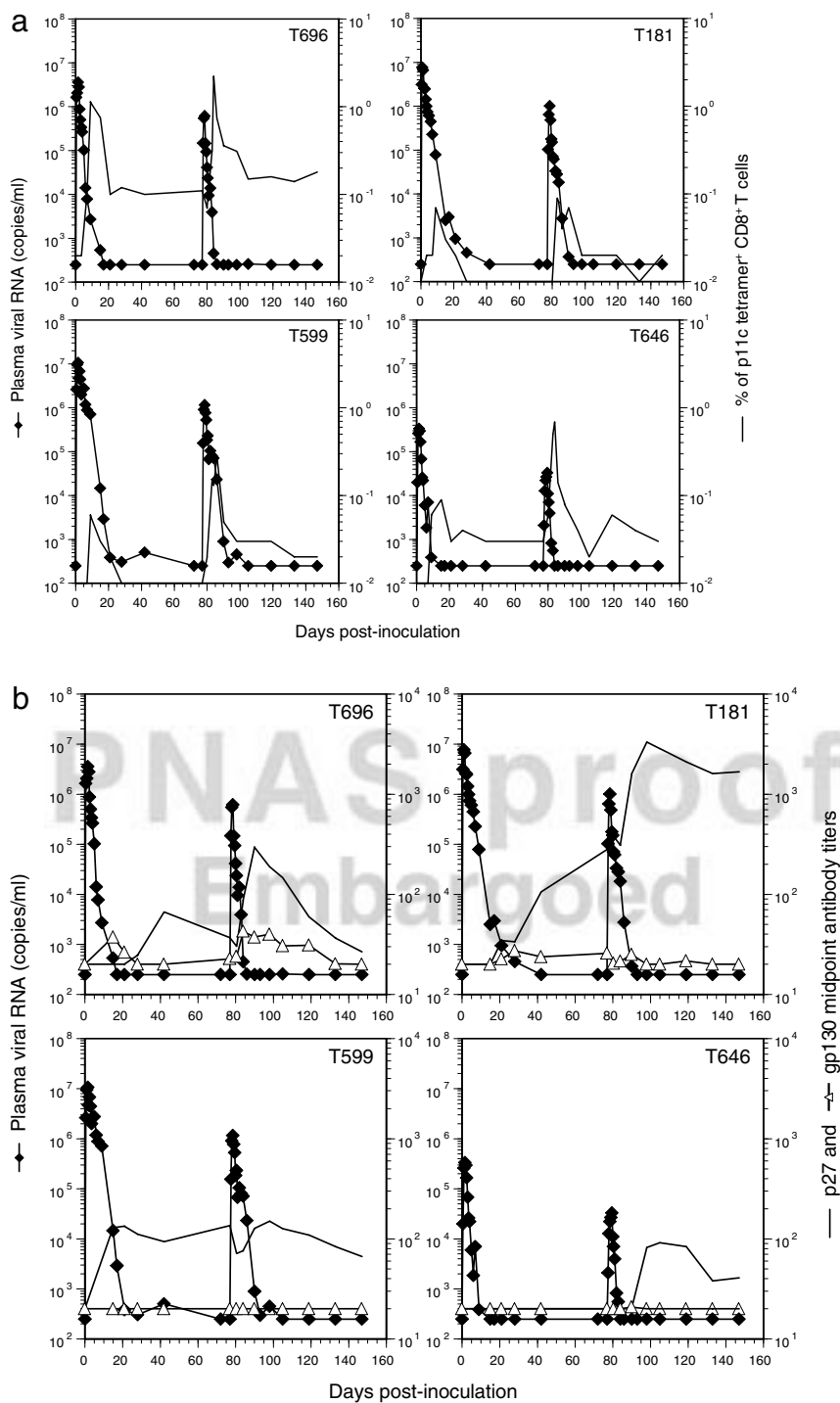
**Fig. 2.** Plasma viral loads and specific immune responses after the first and second inoculations of scSIV-infected PBMCs. SIV RNA levels in the plasma were measured by real-time PCR using SIV *gag*-specific primers and a molecular beacon. The detection limit of the assay was ≈250 copies per ml. (*a*) SIV-specific CTL responses to the p11c epitope of SIV Gag were determined by tetramer staining. (*b*) Antibody responses to SIV p27 and gp130 were measured by ELISA.

(19). Without considering the possibility of superinfections, the number of infected cells could have been overestimated and resulted in an underestimate of the SIV burst size.

Fourth, our calculation of the SIV burst size was based on prior knowledge of the virion clearance rate, *c*. Here, a conservative estimate based on our plasma apheresis experiments in humans (8) was used to analyze the data. Larger estimates of *c* have been obtained from either bolus infections or steady infusions of SIV virions into rhesus macaques (7). If this larger value of *c* were used,

an even higher estimate of the burst size would have then been obtained.

Our findings suggest that the SIV burst size *in vivo*, and by inference the HIV burst size, is much larger than the previous estimates of $10^2$ to $10^3$ virions per cell (1, 3, 5, 6). Interpreted in conjunction with the rates of virion clearance and cell death, the burst size estimates presented here may be used to determine the total number of productively infected cells in an infected individual when the plasma viral load is known. With the burst size almost two
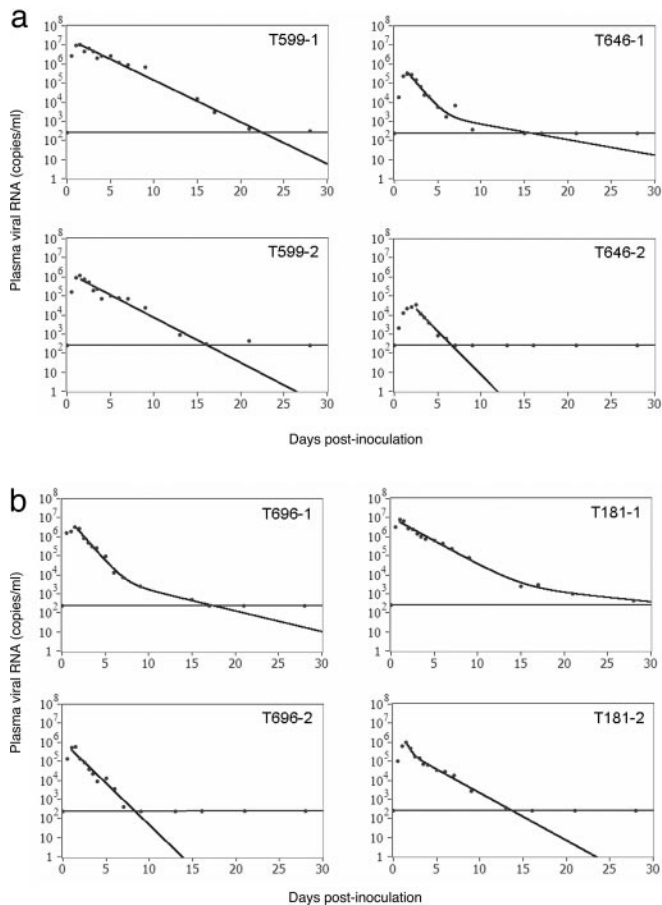
**Fig. 3.** Decay curves of scSIV-infected PBMCs. Plasma viral load data were fitted by using a nonlinear least-square method to determine the decay rate of productively infected cells. The best-fit theoretical curves to the viral load changes are presented. After the peak of viremia, viral load decays adhered to either a two-phase or a single-phase decay model as determined by the *F* test, a statistical test that compares the ''goodness'' of fit between the two models. The horizontal line through each graph indicates the detection limit of the real-time RT-PCR assay ($\approx$250 copies per ml).

orders of magnitude higher than previous estimates, the dynamics of the steady-state relationship indicate that the number of productively infected cells must then be two orders of magnitude lower. Although the exact number and tissue locations of productively

**Table 2. Potential impact of various confounders on estimates of viral burst size**

| | Possible impact on virion burst size | |
|---|---|---|
| Confounders | Overestimate | Underestimate |
| scSIV with VSV-G env* | | √ |
| SEB activation[†] | √ | √ |
| Superinfection | | √ |
| Virion clearance rate (c)[‡] | | √ |

*Underestimate of the true burst size can derive from an overestimate of the number of infected cells, $I_0$* from Eq. **1** as it is expected from the multitropic nature of scSIV with VSV-G ENV or from the assumption of absence of superinfection from *ex vivo* infection of PBMCs.

[†]SEB infection can lead to either an underestimate or overestimate of $I_0$*, which consequently generates an underestimate and overestimate, respectively, of the true burst size.

[‡]Virion clearance rate is a conservative estimate of the true SIV clearance rate (7) and leads to an underestimate of the true burst size from Eq. **8**.

infected cells are currently unknown, it is likely to be concentrated in the gastrointestinal tract where higher levels of activation and higher numbers of lymphocytes have been identified. This finding also raises the interesting question of why more CD4^{+} T cells are not productively infected.

In summary, we have estimated the SIV burst size *in vivo* by using scSIV to inoculate rhesus macaques by *ex vivo* infection and i.v. reinfusion of autologous PBMCs. Based on a simple mathematical model, the viral burst size was calculated to be $\approx 5 \times 10^4$ virions per infected cell. This *in vivo* viral burst size estimate has been computed in a controlled manner that eliminates the confounding effects of subsequent viral spread and production. A more thorough understanding of the SIV and HIV burst size *in vivo* and other dynamic viral and cellular parameters may better guide the design of strategies that reduce the number of virions produced and thereby limit, if not prevent, the occurrence of continued infections.

## Methods

**Rhesus Macaques.** All rhesus macaques (*Macaca mulatta*) were screened for SIV, HIV-2, simian type D retrovirus, and simian T cell lymphotropic virus type 1 infections and the Mamu-A*01 MHC class I phenotype according to previously established methods (20, 21). Each macaque was housed in a single animal cage at the Tulane Regional Primate Research Center in New Orleans. Approval for the animal protocols was obtained from the Institutional Animal Care and Use Committee.

**Sample Collection.** Peripheral blood samples were drawn and separated into plasma and PBMCs. Plasma samples were stored at $-80°$C. PBMCs were pelleted and frozen at $-80°$C or frozen viably at $-150°$C in freezing media [50% RPMI medium 1640, 40% FBS, and 10% DMSO (Sigma-Aldrich)].

**Quantifying SIV RNA in Plasma and Proviral DNA in PBMCs by Real-Time PCR.** Plasma viral RNA and PBMC proviral DNA were quantified as described (22) by real-time PCR using a molecular beacon to detect copies of SIV *gag*. The assay sensitivity for SIV RNA was $\approx$250 RNA copies per ml of plasma, whereas that for proviral DNA was 10 input copies. To determine the number of proviral DNA per cell, copy numbers of the rhesus *CCR5* gene in each PBMC sample were also quantified as described (23).

**Tetramer Staining.** SIV Gag-specific CD8^{+} T cells were measured by using the phycoerythrin-labeled p11C Gag tetramer (24) obtained from ●●● Letvin and ●●● Kuroda through the AIDS Research and Reference Reagent Program at the National Institutes of Health. PBMCs from Mamu-A*01 macaques with known binding to the p11C Gag tetramer were used as the positive control.

**SIV p27 and gp130 Antibody ELISA.** Antibodies to SIV p27 and gp130 in the plasma were measured by ELISA (25) as described. For the detection of p27 antibodies, a p27-GST fusion protein was prepared from an expression plasmid (provided by Ian Jones, University of Reading, Reading, U.K.) and purified on a GST column (Amersham Biosciences). For the detection of gp130 antibodies, an antibody capture ELISA was performed with a sheep anti-SIV-gp130 polyclonal antibody (D7369; International Enzymes). The gp130 antigen was produced by the CHO-SIVmac239 gp130 cell line (AIDS Research and Reference Reagent Program at the National Institutes of Health).

**Construction of scSIV Expression Plasmid.** SIVΔenv, which comprises the SIVmac239 genome with a deletion at the 5′ end of the *env* gene, was constructed by PCR mutagenesis. Specifically, an amplicon with a 415-bp deletion was generated by PCR with primer pairs that anneal to the pathogenic SIVmac239 in a discontinuous fashion. Sequences between the annealed regions were precisely deleted during the PCR amplification. Using appropriate restric-

tion enzymes, the wild-type sequence was replaced by the resultant amplicon to generate SIVΔenv. The SIVΔenv plasmid was amplified in MAX EFFICIENCY STBL2 competent cells (Invitrogen) that were grown at 30°C. Correct sequence and orientation were confirmed by restriction enzyme digestion and DNA sequencing. An additional plasmid, VSV-G (provided by Nathaniel Landau, The Salk Institute for Biological Studies, La Jolla, CA), which contains the glycoprotein from the VSV, was used to generate scSIV through pseudotyping.

**Generation of scSIV.** scSIV was generated by transient transfection of 293T cells with the SIVΔenv and the VSV-G plasmids by calcium phosphate precipitation (CellPhect; Amersham Biosciences) according to the manufacturer's instructions. Approximately 5 h posttransfection, the cells were washed with DMEM to remove residual DNA complexes and replenished with fresh complete DMEM. Culture supernatants were collected from the plates at 24 and 48 h posttransfection. After filtration through a 0.2-$\mu$m filter unit (Corning), the supernatants were stored at −80°C. Transfected 293T cells were harvested at 48 h posttransfection. Collected cell pellets and culture supernatants were used to prepare cell and virion lysates for Western blot analysis.

**Purification and Titration of scSIV.** Filtered transfection supernatants collected at both 24 and 48 h posttransfection were layered on top of a 32% glycerol cushion in a polyallomer ultracentrifuge tube (Beckman Coulter). Ultracentrifugation was performed in an SW28 rotor (Beckman Instruments) at 28,000 rpm and 4°C for ≈2 h. After the spin, the supernatants were carefully aspirated off. Pelleted virion particles were resuspended in 300 $\mu$l of PBS for 1 h at 4°C and then stored at −80°C. After multiple rounds of cotransfection followed by virus concentration, the entire batch of concentrated virus was pooled together, redistributed in 1-ml aliquots, and titered on B3 indicator cells (provided by Zhiwei Chen, Aaron Diamond AIDS Research Center), a derivative of the HeLa cell line. In addition to expressing the human *CD4* and the rhesus macaque *CCR5* genes, the B3 cell line also contains a $\beta$-galactosidase reporter gene that is under the control of the HIV-1 LTR. After SIV infection, the production of a functional Tat protein transactivates the HIV-1 LTR and triggers the expression of $\beta$-galactosidase. As a result, infected cells stain blue in the presence of X-gal. Infectious titers were calculated by multiplying the total number of blue cells per well by the dilution factor and normalizing to 1 ml. At low MOI, one blue cell was assumed to equal one infectious virion particle, or one cell infectious dose.

***Ex Vivo* Infection and i.v. Reinfusion.** Four SIV-naïve rhesus macaques with the Mamu-A*01 MHC class I phenotype (T696, T181, T599, and T646) were experimentally inoculated with scSIV particles by *ex vivo* infection and i.v. reinfusion. In detail, ≈1.3 to 4.0 × 10⁷ PBMCs from 20 ml of blood were isolated from each monkey and stimulated *in vitro* with 4 $\mu$g per ml of SEB (Sigma-Aldrich). After stimulation for 2.5 days, traces of SEB were removed from the PBMCs by extensive washing, which entailed resuspending and pelleting the cells with PBS at least six times. The activated cells were then exposed to scSIV at an MOI of 3.0 or 9.2, as titered on the B3 cell line, in RPMI medium 1640 supplemented with 2,000 units. of recombinant IL-2 (provided by Chiron). After ≈16 h, residual extracellular scSIV was removed by extensive washing with PBS as before. The number of virus-exposed cells that were still viable was counted. A small aliquot of these cells was reserved to estimate the fraction of cells infected. The remaining *ex vivo*-infected cells were then pelleted to ≈2 ml for autologous reinfusion by i.v. injection. Before inoculation, 5 ml of blood from each monkey was collected to establish baseline conditions.

Blood was collected from each animal every 12 h during the first 3 days, daily for the remainder of the first week, and then weekly thereafter. Plasma and cells were separated and stored at −80°C

and −150°C, respectively, immediately after collection during the first week after each inoculation. For all subsequent weeks, plasma and cells were separated 1 day after collection. The entire procedure of *ex vivo* infection and i.v. reinfusion of infected cells was repeated several weeks later with an MOI ranging from 3.1 to 12.6.

**Viral Dynamic Model.** In the experiment, a given number of cells, $I^*_0$, infected with scSIV was infused into uninfected rhesus macaques. Assuming that multiple cell populations were productively infected (11), the amount of virus produced by the shorter and the longer-lived infected cells can be modeled by the following equations (26):

$$\frac{dT^*}{dt} = -\delta T^*$$

$$\frac{dM^*}{dt} = -\mu M^* \qquad [1]$$

$$\frac{dV}{dt} = N\delta T^* + pM^* - cV,$$

where $T^*$ is the density of shorter-lived productively infected cells, $\delta$ is their death rate, $V$ is the viral load, $c$ is the virion clearance rate, and $N$ is their burst size. In addition, $M^*$ is the density of the longer-lived infected cells, which die with rate $\mu$ per cell and produce virus at rate $p$ per cell.

Because new infections were not possible after infusion with scSIV-infected cells, $T^*$ and $M^*$ decayed according to:

$$T^*(t) = T^*(0)e^{-\delta t}$$
$$M^*(t) = M^*(0)e^{-\mu t} \qquad [2]$$

and the viral load, $V(t)$, changed according to:

$$V(t) = \frac{N\delta T^*(0)}{c-\delta}(e^{-\delta t} - e^{-ct}) + \frac{pM^*(0)}{c-\mu}(e^{-\mu t} - e^{-ct}). \quad [3]$$

Therefore, in this model of single-cycle infection, $V(t)$ can be shown to rise from zero, reach a maximum, and then decline. With the rate of virion clearance, $c$, considerably faster than the rates of infected cell death, $\delta$ and $\mu$, the change in viral load, $V(t)$, during the postpeak decline can be represented by:

$$V(t) \cong (N\delta T^*(t_{pk})e^{-\delta(t-t_{pk})} + pM^*(t_{pk})e^{-\mu(t-t_{pk})})/c, \quad [4]$$

where $t_{pk}$ is the time at which the peak viral load was attained. Because $T^*(t_{pk})$ and $M^*(t_{pk})$ are not known, we rewrote this equation as

$$V(t) \cong V(t_{pk})(Ae^{-\delta(t-t_{pk})} + (1-A)e^{-\mu(t-t_{pk})}), \quad [5]$$

where $A = N\delta\ T^*(t_{pk})/[N\delta\ T^*(t_{pk}) + pM^*(t_{pk})]$ is an unknown parameter that needs to be estimated from the data.

The parameter $A$ and the turnover rates of the shorter and the longer-lived productively infected cells, $d$ and $\mu$, respectively, were estimated by fitting the logarithm of the viral load data after the peak to the logarithm of Eq. **5** by using a nonlinear least-square procedure. The time at which the viral load peak occurred was scaled to zero for the analysis. From the best-fit values of $\delta$ and $\mu$, the half-lives of the shorter-lived population, $t_{½,\delta} = ln2/\delta$, and the longer-lived population, $t_{½,\mu} = ln2/\mu$, were calculated. A bootstrapping procedure (27, 28) was used to compute the 95% confidence intervals for each parameter estimate. A single-phase viral decay is described by Eq. **4** when $M^*$, the density of the longer-lived infected cells dying with rate $\mu$ per cell, is assumed to be negligible. In this case, the last term on the right side of Eq. **5** is eliminated. To determine whether a single-phase or a two-phase decay model was more appropriate, an $F$ test on the residual sum of squares

MEDICAL SCIENCES

normalized by the appropriate degrees of freedom using a significance level, $\alpha$, equal to 0.05 was performed.

**Viral Burst Size.** The change in viral load over time reflects the number of virions produced and cleared within that time. Mathematically, this may be expressed as a differential equation:

$$\frac{dV(t)}{dt} = P(t) - cV(t), \qquad [6]$$

where $P(t)$ represents the rate of virion production by both the shorter and the longer-lived infected cells at time $t$ and $cV(t)$ represents the rate of virion clearance at time $t$, as determined by the product of the number of virions at time $t$, $V(t)$, and the viral clearance rate per virion, $c$.

From the area under the viral load curve, one can estimate the average *in vivo* burst size, $N$. Using this area under the curve (AUC) approach, the total number of virions produced and cleared is determined by integrating both sides of Eq. **6**:

$$\int_0^\infty \frac{dV(t)}{dt}dt = V(\infty) - V(0) = \int_0^\infty (P(t) - cV(t))dt.$$

Considering that there was no virus initially in the animal and that all scSIV-infected cells and the virions they produced were eventually eliminated, both $V(\infty)$ and $V(0)$ should equal zero. Therefore, the total number of virions produced should equal the total number of virions cleared:

$$\int_0^\infty P(t)dt = c\int_0^\infty V(t)dt = cAUC, \qquad [7]$$

where $AUC$ represents the area under the curve of $V(t)$. In addition, the total number of virions produced is $NI^*_0$, i.e., the product of the average number of virions produced per cell, $N$, and the total number of infected cells put into the animal, $I^*_0 = T^*(0) + M^*(0)$. Thus, the viral burst size can be determined by:

$$N = \frac{cAUC}{I_0^*}. \qquad [8]$$

Here, $I^*_0$ represents all infected cells put into the animal irrespective of whether they are short-lived, $T^*(0)$, or long-lived, $M^*(0)$.

To obtain the $AUC$, or the total virion production, the viral load data, expressed as SIV RNA copies per ml, was integrated until day 72 postinoculation and then multiplied by a conversion factor of 53 ml of blood per kg of body weight (29). This process yielded a minimal estimate because virions that resided in extravascular spaces and virions that were produced after day 72 were not considered. No measurement of the virion clearance rate, $c$, was made, and the previously determined average value (8), $c = 23$ day$^{-1}$, was adopted. The total number of productively infected cells, $I^*_0$, was estimated from the real-time PCR of proviral SIV *gag* copies in a small portion of the virus-inoculated PBMCs reserved immediately before inoculation. Assuming that no superinfection occurred, each detected copy of SIV *gag* represented one infected cell. If all such cells were not productively infected then $I^*_0$ is overestimated and the burst size, $N$, is underestimated.

1. Dimitrov DS, Willey RL, Sato H, Chang, L-J, Blumenthal R, Martin MA (1993) *J Virol* 67:2182–2190.
2. Eckstein DA, Penn ML, Korin YD, Scripture-Adams DD, Zack JA, Kreisberg JF, Roederer M, Sherman MP, Chin PS, Goldsmith MA (2001) *Immunity* 15:671–682.
3. Tsai WP, Conley SR, Kung HF, Garrity RR, Nara PL (1996) *Virology* 226:205–216.
4. Chun, T-W, Carruth L, Finzi D, Shen X, Digiuseppe JA, Taylor H, Hermankova M, Chadwick K, Margolick J, Quinn TC, et al. (1997) *Nature* 387:183–188.
5. Haase AT, Henry K, Zupancic M, Sedgewick G, Faust RA, Melroe H, Cavert W, Gebhard K, Staskus K, Zhang, Z-Q, et al. (1996) *Science* 274:985–989.
6. Hockett RD, Kilby JM, Derdeyn CA, Saag MS, Sillers M, Squires K, Chiz S, Nowak MA, Shaw GM, Bucy RP (1999) *J Exp Med* 189:1545–1554.
7. Zhang L, Dailey PJ, He T, Gettie A, Bonhoeffer S, Perelson AS, Ho DD (1999) *J Virol* 73:855–860.
8. Ramratnam B, Bonhoeffer S, Binley JM, Hurley A, Zhang L, Mittler JE, Markowitz M, Moore JP, Perelson AS, Ho DD (1999) *Lancet* 354:1782–1785.
9. Nowak MA, Lloyd AL, Vasquez GM, Wiltrout TA, Wahl LM, Bischofberger N, Williams J, Kinter A, Fauci AS, Hirsch VM, Lifson JD (1997) *J Virol* 71:7518–7525.
10. Mittler JE, Markowitz M, Ho DD, Perelson AS (1999) *AIDS* 13:1415–1417.
11. Perelson AS, Essunger P, Cao Y, Vesanen M, Hurley A, Saksela K, Markowitz M, Ho DD (1997) *Nature* 387:188–191.
12. Bukrinsky MI, Stanwick TL, Dempsey MP, Stevenson M (1991) *Science* 254:423–427.
13. Stevenson M, Stanwick TL, Dempsey MP, Lamonica CA (1990) *EMBO J* 9:1551–1560.
14. Tang S, Patterson B, Levy JA (1995) *J Virol* 69:5659–5665.
15. Zack JA, Arrigo SJ, Weitsman SR, Go AS, Haislip A, Chen IS (1990) *Cell* 61:213–222.
16. Zhang Z, Schuler T, Zupancic M, Wietgrefe S, Staskus KA, Reimann KA, Reinhart TA, Rogan M, Cavert W, Miller CJ, et al. (1999) *Science* 286:1353–1357.
17. Jung A, Maier R, Vartanian, J-P, Bocharov G, Jung V, Fischer U, Meese E, Wain-Hobson S, Meyerhans A (2002) *Nature* 418:144.
18. Vandegraaff N, Kumar R, Burrell CJ, Li P (2001) *J Virol* 75:11253–11260.
19. O'Doherty U, Swiggard WJ, Jeyakumar D, McGain D, Malim MH (2002) *J Virol* 76:10942–10950.
20. Liska V, Lerche NW, Ruprecht RM (1997) *AIDS Res Hum Retroviruses* 13:433–437.
21. Knapp LA, Lehmann E, Piekarczyk MS, Urvater JA, Watkins DI (1997) *Tissue Antigens* 50:657–661.
22. Jin X, Bauer DE, Tuttleton SE, Lewin S, Gettie A, Blanchard J, Irwin CE, Safrit JT, Mittler J, Weinberger L, et al. (1999) *J Exp Med* 189:991–998.
23. Arron ST, Ribeiro RM, Gettie A, Bohm R, Blanchard J, Yu J, Perelson AS, Ho DD, Zhang L (2005) *Eur J Immunol* 35:46–55.
24. Kuroda MJ, Schmitz JE, Barouch DH, Craiu A, Allen TM, Sette A, Watkins DI, Forman MA, Letvin NL (1998) *J Exp Med* 187:1373–1381.
25. Connor RI, Montefiori DC, Binley JM, Moore JP, Bonhoeffer S, Gettie A, Fenamore EA, Sheridan KE, Ho DD, Dailey PJ, Marx PA (1998) *J Virol* 72:7501–7509.
26. Perelson AS, Neumann AU, Markowitz M, Leonard JM, Ho DD (1996) *Science* 271:1582–1586.
27. Efron B, Tibishinari RJ (1993) in *An Introduction to the Bootstrap*, ed Cox DR (Chapman & Hall, New York), pp 105–123.
28. Efron B, Tibishinari RJ (1993) in *An Introduction to the Bootstrap*, ed Cox DR (Chapman & Hall, New York), pp 45–49.
29. Salvato MS, Rater M, Pauza CD (1996) *J Med Primatol* 25:112–121.